LORIS: A Lightweight Free-Climbing Robot for Extreme Terrain Exploration

Paul Nadan[1], Spencer Backus[2], and Aaron M. Johnson[3]

***Abstract*— Climbing robots can investigate scientifically valuable sites that conventional rovers cannot access due to steep terrain features. Robots equipped with microspine grippers are particularly well-suited to ascending rocky cliff faces, but most existing designs are either large and slow or limited to relatively flat surfaces such as walls. We present a novel free-climbing robot to bridge this gap through innovations in gripper design and force control. Fully passive grippers and wrist joints allow secure grasping while reducing mass and complexity. Forces are distributed among the robot's grippers using an optimization-based control strategy to minimize the risk of unexpected detachment. The robot prototype has demonstrated vertical climbing on both flat cinder block walls and uneven rock surfaces in full Earth gravity.**

I. Introduction

Climbing robots have the potential to explore steep cliff faces, caves, and microgravity environments of scientific interest throughout the solar system [1–4]. While wheeled rovers are typically limited to shallow slopes, robots equipped with microspine grippers (summarized in Table I) are capable of ascending steep rock faces using arrays of sharp hooks that catch on small asperities in the surface [5,6]. The earliest microspine grippers were fully passive, relying on the weight of the robot to provide the necessary engagement force, and robots equipped with these grippers were designed to traverse relatively flat surfaces such as the walls of buildings [7–9].

In contrast, the microspine gripper in [10] used an actuator to generate large, opposing engagement forces between its microspines, enabling the LEMUR series robots [10,11] to support their greater weight and traverse unstructured natural terrain features. Other researchers have followed a similar approach, creating active grippers that operate on the same principle, but with increased engagement speed and reduced size and mass [12,13]. Some grippers can close around protruding footholds to provide a robust grasp, but are less effective on a flat surface [14–16].

In [17], the authors present an insect-inspired strategy called directed inward grasping (DIG), in which opposed engagement forces are generated between the legs of a climber rather than by each gripper individually. This allows passive grippers to obtain many of the same benefits as active grippers, but without the additional mass and complexity. However, the robot in [17] uses a single hook per foot, limiting it to climbing on a mesh screen.

Fig. 1: The LORIS robot uses passive microspine grippers and directed inward grasping to ascend the side of a tufa stone bridge.

Despite the demonstrated successes of these robots, climbing remains an inherently high-risk operation, and the premature demise of a primary mission asset during a space mission would be catastrophic. Instead, one or more small, expendable climbing robots could be carried alongside a larger conventional rover, to be deployed at sites of scientific interest without endangering the primary mission objectives. Such a system would reduce overall risk, enable division of labor between multiple vehicles, and be more likely to be deployed as the first climbing robot in space. However, this requires a robot that is both lightweight and capable of climbing on unstructured terrain.

In this work, we present a novel passive gripper design capable of supporting varying lateral loads along with a robot prototype, the Lightweight Observation Robot for Irregular Slopes (LORIS), that can ascend unstructured steep and vertical terrain (Fig. 1). We further present an optimization-based force control strategy to maximize gripper adhesion by generating DIG forces. We provide climbing experiments on uneven slag and vesicular basalt climbing walls, flat cinderblock, and natural rock features. LORIS is to our

This work was supported by a NASA Space Technology Graduate Research Opportunities Award. A portion of this research was carried out at the Jet Propulsion Laboratory, California Institute of Technology, under a contract with the National Aeronautics and Space Administration (80NM0018D0004).

[1]Robotics Institute, [3]Mechanical Engineering, Carnegie Mellon University, Pittsburgh, PA 15213, USA, {pnadan, amj1}@andrew.cmu.edu

[2]Jet Propulsion Laboratory, California Institute of Technology, 4800 Oak Grove Drive M/S 82-105, spencer.backus@jpl.nasa.gov

Robot	Terrain	DoF (per limb)	Mass (kg)	Speed (m/min)	Gravity (g)
RiSE [7]	Flat Walls	2	3.8	15	1
HubRobo [14]	Handholds	3	3.0	0.17	0.38
SCALER [15]	Handholds	6	6.3	0.35	1
LEMUR 2B [10]	Irregular	3	10	Unknown	1
LEMUR 3 [11]	Irregular	7	35	0.0027	0.38
RockClimbo [12]	Irregular	4	3.5	0.14	0.67
LORIS	**Irregular**	**3**	**3.2**	**0.20**	**1**

TABLE I: Comparison to Prior Work

knowledge the first robot to generate DIG forces using microspines and at 3.2 kg the first robot of its size to demonstrate free-climbing on irregular vertical rock faces in full Earth gravity.

II. Robot Design

LORIS is a quadrupedal robot with three joint actuators per limb for the shoulder, "wing" (abduction/adduction), and knee. While wall-climbing robots like RiSE only required two actuators per limb to climb on flat surfaces [7], the third limb joint provides the robot more freedom to select footholds as needed on irregular terrain. At the end of each limb is a passive microspine gripper on a passive 3-degree of freedom (DoF) wrist. This design is analogous to ground quadrupeds that have 3-DoF legs with 3 passive DoF at their point feet, enabling arbitrary positioning and orienting of the body. Compliant degrees of freedom within both the gripper and the wrist provide "mechanical intelligence", the ability to naturally conform to uneven terrain without any actuation or control. A pitch spine actuator in the body aids in traversing larger obstacles and plane transitions, as in [18,19], and a tail actuator is used to push against the surface with a large moment arm, reducing the adhesive force needed by the front grippers when climbing.

A. Splayed Microspine Gripper

Microspines rely on a steep angle of attack relative to the contact surface, typically around 70° [8]. Due to this directionality, they are not effective at individually resisting lateral loads. While climbing flat walls rarely requires variation in the load direction, more complicated terrain requires grippers that can support loads over a wider range of directions without repositioning. Active grippers avoid this limitation by placing microspines in a ring, so that a subset of them are always oriented to oppose the external load [10,14]. However, this approach inherently requires some form of actuation to engage or release the grasp.

Instead, we propose a passive gripper with a single pair of splayed carriages angled $\pm 45°$ to the gripper axis (Fig. 2a). These carriages in combination can apply loads with tangential ($+x$) and lateral ($\pm z$) components as force is distributed into one component along each carriage's axis. The gripper is fully passive and can be disengaged by unloading tangentially, as this direction of motion is not opposed by any microspines. Unlike an active gripper it cannot support negative tangential or purely lateral loads, but in practice the need to resist the pull of gravity or generated DIG forces will create a significant positive tangential component.

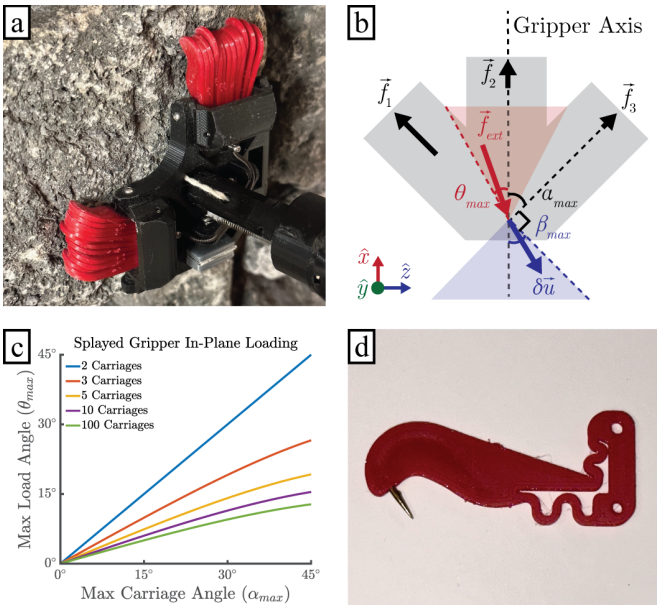

Fig. 2: a) A splayed microspine gripper engaged with a rock. b) A free-body diagram of a 3-carriage splayed gripper, showing viable displacements in blue and viable loading in red. Angles are defined relative to the gripper axis. c) A plot of the maximum loading angle for varying gripper carriage geometry. d) A 3D-printed microspine with an embedded fishhook and serpentine flexures.

There are many possible splayed gripper designs, depending on the number and splay angle of the carriages. To find the optimum in this design space, we model the in-plane forces each carriage experiences during static loading (Fig. 2b). The n microspine carriages are assumed to act as linear springs with stiffnesses k_i oriented at angles α_i. If the gripper translates by a small displacement δu along the angle β, then the resulting tangential carriage force f_i^t and net in-plane external force $\vec{f}_{ext}^{xz}$ are given by,

$$f_i^t = k_i \cos(\beta - \alpha_i)\delta u \tag{1}$$

$$f_{ext}^{xz} = -\sum_{i=1}^{n} f_i^t \begin{bmatrix}\cos(\alpha_i)\\ \sin(\alpha_i)\end{bmatrix} \tag{2}$$

If any carriage experiences a displacement in the opposite direction of its microspines, then that carriage loses engagement and the grasp is considered to have failed. This occurs when $\cos(\beta - \alpha_i) < 0$, thus β is bounded by $[\alpha_{max} - 90°, -\alpha_{max} + 90°]$. Computing θ, the angle of $\vec{f}_{ext}$ relative to the gripper axis, at these bounds produces the minimum and maximum loading angles $-\theta_{max}$ and θ_{max} that the gripper can support.

In Fig. 2c, the maximum loading angle θ_{max} is plotted for symmetric grippers with different numbers of evenly spaced, equal stiffness carriages as a function of carriage angle α_{max}. Two carriages outperform larger numbers because additional intermediary carriages increase the relative u component of the load without affecting the bounds of β. At α_{max} values greater than approximately $45°$ the angle of the outermost spines becomes too steep to effectively catch on asperities during initial engagement.

B. Passive Wrist Joint

Full control over the gripper's orientation in space would require three additional actuators per limb, but significant mass reduction is possible by letting those degrees of freedom remain passive. We define rotations with pitch about the z axis (i.e. rotating up-down), roll about the x axis (left-right), and yaw about the y axis (counterclockwise-clockwise). To remove the dependence of the limb kinematics on the potentially unknown gripper orientation, we let all three axes of rotation intersect at a common point. Mechanically, $\pm 35^\circ$ of pitch and roll are provided by a ball joint while the yaw degree of freedom is supplemented by a low-friction 360° revolute joint.

The gripper must make contact at 3 or more points to passively align itself with the climbing surface in the pitch and roll axes. For the splayed gripper design above, these are ideally the two sets of microspines and a contact point at the base of the gripper. On highly convex features this may not be the case, potentially causing a grasp failure. Furthermore, when these axes are passive the gripper performance becomes sensitive to the location of the center of rotation.

We model the gripper in terms of the width between the two carriages w, the height between the microspines and the base contact h, the splay angle α, and the center of rotation $\vec{p}$ (Fig. 3). Assuming static equilibrium and a frictionless base contact, the system equations,

$$0 = f^x_{ext} + (f^t_1 + f^t_2)\cos(\alpha) \tag{3}$$
$$0 = f^z_{ext} + (f^t_2 - f^t_1)\sin(\alpha) \tag{4}$$
$$0 = f^y_{ext} + f^n_1 + f^n_2 + f^y_b \tag{5}$$
$$0 = \tau^x_{ext} + \frac{w}{2}(f^n_1 - f^n_2) + p^y f^z_{ext} \tag{6}$$
$$0 = \tau^z_{ext} + h(f^n_1 + f^n_2) + p^x f^y_{ext} - p^y f^x_{ext} \tag{7}$$

can be solved analytically for the forces at the microspines $\vec{f_1}$, $\vec{f_2}$ and the base contact f^y_b in terms of the gripper geometry and the external force $\vec{f}_{ext}$ and torque $\vec{\tau}_{ext}$.

The resulting forces should obey two constraints to prevent the gripper from disengaging: 1) the pull-off force angle on the microspines cannot exceed a threshold ϕ_{slip}, as found by [20], and 2) the required normal force on the base contact cannot be negative (or else the gripper pitches downward, causing the spine angle of attack to become too steep),

$$-f^n_1 \leq f^t_1 \tan(\phi_{slip}) \tag{8}$$
$$-f^n_2 \leq f^t_2 \tan(\phi_{slip}) \tag{9}$$
$$0 \leq f^y_b \tag{10}$$

Focusing on the pitch axis and assuming no torque at the joint, let $f^z_{ext} = 0$, $\tau^x_{ext} = 0$, and $\tau^z_{ext} = 0$, then solve the constraints numerically to compute the maximum feasible gripper pull-off force angle ϕ_{max} given the pivot location. That maximal angle is plotted in Fig. 3, which shows that the optimal pivot location lies roughly along a line. Intuitively, moving the pivot further from the surface results in greater spine pull-off force, while moving the pivot toward the surface causes the gripper to begin rotating at a smaller loading angle. Thus the pivot point should be in line with the spine contact force vector at the gripper's maximum loading angle to minimize both effects. However, due to space constraints the pivot could not be placed as close to the surface as optimal, and so a pair of springs were added to provide a negative preload torque τ^z_{ext}. This shifts the optimum away from the surface, although the exact size of the shift depends on the applied force magnitude.

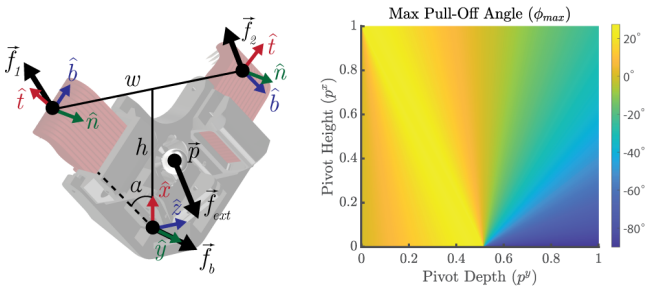

Fig. 3: Left: an annotated image of a splayed gripper, with the three contact points and the pivot ball joint indicated by circles. Right: a plot of the maximum pull-off force angle relative to the wall as function of the pivot joint location for a 2-carriage gripper with a $\pm 45^\circ$ splay angle. Pivot height and depth are normalized by the gripper height h.

While the gripper naturally flattens itself against the surface in pitch and roll, the gripper yaw depends on its angle at the moment contact is made. We would like to align the gripper with the nominal in-plane loading direction, which depends on the external gravity vector and any generated internal forces. If the DIG force magnitude is nominally proportional to the gravitational load on each gripper, then the optimal gripper angle is a fixed angular offset from the gravity vector's projection into the surface plane. We can therefore distribute the mass of the gripper such that its minimum-energy yaw angle is equal to this offset, similar to the grippers in [21] (which can be considered to have an offset of zero). A limitation of this approach is the requirement of a significant in-plane gravity component, and thus this strategy does not generalize to fully inverted climbing or micro-gravity environments.

C. Robot Prototype

The LORIS robot, Fig. 4, is designed for ease of manufacturing – all parts are either 3D printed, waterjet from aluminum, or commercially available. The robot body consists of two 2mm-thick aluminum baseplates separated by standoffs. The frame is 315mm long by 180mm wide by 44mm deep and separated into two equal halves, connected by the body joint. The first limb motors project outward from the body to ensure a full range of motion. The limbs are composed of off-the-shelf plastic and custom PLA brackets. The 348 mm tail consists of a carbon fiber tube encased in a rounded PLA shell to easily slide over uneven rocks.

The actuators used are Dynamixel AX18-A servo motors for the wing degree of freedom and tail, and higher torque Dynamixel XM430-W350T servos for the shoulders, knees, and body joint. LORIS can either be powered by an offboard supply or carry a 3S LiPo battery. The robot can also carry an

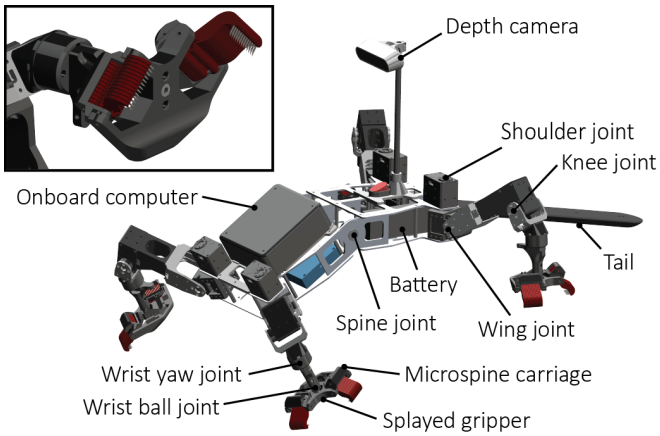

Fig. 4: An annotated visualization of the LORIS robot design, with a splayed gripper enlarged in an inset.

Intel NUC 11 for onboard computation. An Intel RealSense D435i depth camera mounted on a carbon fiber mast allows the robot to construct a map of the upcoming terrain.

The passive grippers are composed of 3D printed PLA. 26 microspines are evenly divided among two carriages forming a 90° angle. The carriages are free to independently rotate toward the surface by up to 30°. This hierarchical compliance aids the gripper in conforming to convex features at a larger scale than an individual spine. Low-stiffness restoring springs ensure that the carriages are pitched downward while making initial contact, but can easily be pressed back when placed on a flatter surface.

The microspines are 3D printed from TPU using the additive manufacturing process in [22] with embedded fishhooks (Fig. 2d). The primary improvement in the design is the removal of the long flexure that rotates the hook into the surface. Instead, a serpentine diagonal flexure is sufficient to provide a similar level of normal compliance, enabling a significant reduction in footprint.

III. Controller Design

The control strategy is divided into three components. The force optimization determines ideal contact forces to minimize the risk of gripper failure. These forces are passed as setpoints to the force feedback controller, which uses current-based feedback from the motors to regulate the contact forces. In parallel, the gait planner carries out a climbing gait based on a state machine.

A. Force Optimization

Prior climbing robots such as [7] have relied on the simple strategy of evenly distributing the gravitational load among the grippers. This can suffice on flat surfaces or for actuated grippers with large amounts of holding force, but may not generalize for passive grippers on unstructured terrain. In contrast, the researchers in [23] formulated a combined locomotion and grasping optimization problem for the SCALER robot, but this approach is slow, requiring multiple minutes to find a new solution and thus unable to react quickly if a gripper begins to slip. Instead, we present an optimization problem that can determine the ideal force distribution in a matter of milliseconds for any robot posture, not just vertical climbing on a flat wall. As an added benefit, this approach automatically generates DIG forces if the grippers are oriented to support them.

The optimization considers the contact forces $\vec{f}_i$ at each gripper divided into tangential, normal, and lateral (binormal) components $[f_i^t, f_i^n, f_i^b]$, as well as the tail normal force f_{tail}^n and the adhesion margin c, defined as the minimum additional normal force required to dislodge a gripper. We focus on quasi-static climbing, so the optimal forces can be computed at each timestep without affecting future timesteps.

The optimization is formulated as a linear program, for which many fast solvers exist, which aims to maximize the adhesion margin c given several linear constraints,

$$\underset{\vec{f}_i, f_{tail}^n, c}{\arg\max} \quad c \tag{11}$$

$$\text{s.t. } 0 = \sum_{i=1}^{N} R_i \vec{f}_i + R_{tail}\vec{f}_{tail} + \vec{f}_g \tag{12}$$

$$0 = \sum_{i=1}^{N} \vec{r}_i \times R_i \vec{f}_i + \vec{r}_{tail} \times R_{tail}\vec{f}_{tail} \tag{13}$$

$$f_{min} \leq f_i^t \leq f_{max} \tag{14}$$

$$-f_i^t \tan(\theta_{max}) \leq f_i^b \leq f_i^t \tan(\theta_{max}) \tag{15}$$

$$-f_i^n - f_i^t \tan(\phi_{max}) + c \leq 0 \tag{16}$$

$$0 \leq f_{tail}^n \tag{17}$$

The first two constraints (12)–(13) represent the static equilibrium condition, where the R_i matrices rotate from the gripper frame to the center of mass (CoM) frame, $\vec{r}_i$ are the gripper position vectors in the CoM frame, and $\vec{f}_g$ vector is the gravitational force vector (which can be estimated by summing the current contact force estimates). (14) ensures that the microspines are neither disengaged nor overloaded tangentially. (15) ensures that the in-plane loading angle does not exceed θ_{max}, and (16) ensures that the pull-off angle does not exceed ϕ_{max} out-of-plane. The adhesion margin c is used as a slack variable, representing the minimum safety margin or maximum constraint violation across all grippers depending on its sign. Lastly, we constrain the tail normal force to be non-negative (17).

In Fig. 5, example force solutions are shown for the LORIS robot in a nominal climbing gait with four variations of the gripper design. Non-splayed grippers, able to exert force only along the tangential axis, produce significantly lower adhesion margins even when the grippers are oriented $45°$ inwards to allow for DIG. With splayed grippers, however, this inward angle offset enables the generation of large DIG forces to double the adhesion margin.

One potential future application of this optimization procedure is in foothold planning, to quickly estimate the adhesion margin after placing a gripper at a certain location. Similarly, this optimization can be used as a tool when developing the design and gait of a new robot, allowing a designer to quickly estimate the expected motor torques (via the limb Jacobian)

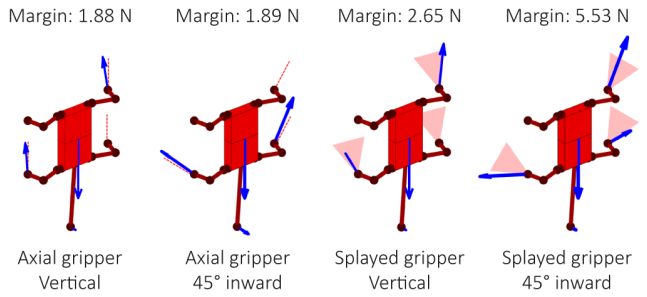

Fig. 5: Optimal force distributions for LORIS's typical climbing posture with the front left limb in swing phase. Adhesion margin is compared between non-splayed (axial) vs splayed grippers, both with and without a 45° inward angle offset. Viable in-plane loading directions for each gripper type are annotated in red.

and adhesion margin for a given morphology and climbing posture.

B. Force Control

LORIS can estimate its current motor torques using the built-in current sensing that Dynamixel servos provide. A moving average filter is used to reduce the noise of these measurements. The limb Jacobian J_i then maps these into contact force estimates, $\hat{f}_i = J_i^{-T}\hat{\tau}_i$.

Given stacked vectors of optimal contact forces F^* and current estimates $\hat{F}$, we could use proportional feedback control to displace each gripper in the opposite direction of the force error and generate a reaction force, i.e. $\delta X = -k_p(F^* - \hat{F})$. However, if the force estimates are not perfectly accurate then the body pose drifts over time. This can be addressed using the grasp map G (the mapping from the contact forces F to the body wrench $\vec{w}$) [24, Sec. II.E]. By projecting the force error into the null space of G, we avoid creating any net wrench on the body while still allowing internal displacements between grippers. This null space projection is accomplished by the matrix $A = I - G^T \text{pinv}(G^T)$, which has the property that $GA\delta X = 0$ for all X. The resulting control law is then,

$$\delta X = -(I - G^T \text{pinv}(G^T))k_p(F^* - \hat{F}) \tag{18}$$

C. Climbing Behaviors

The climbing gait is defined by a simple state machine and relies on proprioception to detect gripper contact and engagement with the surface, providing robustness to uneven terrain without requiring external sensing.

1) **Unload** – constrain the contact force on the gripper $\vec{f}_i$ to be zero in the force optimization and wait for the contact force to converge to the new setpoint.
2) **Disengage** – free the microspines from the surface and raise the gripper until it reaches the maximum height above the surface.
3) **Swing** – translate the gripper to the next foothold.
4) **Engage** – lower the gripper toward the surface until a force threshold is reached, then translate gripper tangentially until a second force threshold is reached.
5) **Load** – remove the constraint on the gripper contact force and wait for convergence.

The disengage state is of particular importance, especially on surfaces with large vesicles (cavities formed by trapped gas during cooling). In this state, the robot attempts to disengage the gripper carriages by translating in the opposite direction to the gripper axis. However, often one carriage comes free before the other, resulting in a lateral load that causes the gripper to yaw. This is addressed by translating the gripper in the direction of the lateral load to reduce it. The second issue is that the grippers sometimes struggle to free their microspines because they are unable to apply a torque with the wrist, so the microspines simply rotate as the gripper tries to pull away. A solution is to lower the gripper back toward the surface whenever a large force into the surface is detected. This reverses the rotation, giving the gripper another chance to work its way free. Additionally, LORIS can react to a gripper snag (unexpected force during swing) or engagement failure (excessive displacement during engagement) by returning to the disengage state, which results in a pawing motion.

The gripper translations are achieved using inverse kinematics, J^{-1}. A teleoperator can also adjust the gripper location during the swing phase to select a desirable foothold, although in the future a footstep planning algorithm may serve this role. The robot's body is kept linearly and angularly centered among the 4 grippers, with a height offset chosen to keep clear of any terrain features.

IV. Experiments

The vertical climbing performance of the LORIS robot was evaluated on several different substrates, including cinderblock, vesicular basalt, and slag (Fig. 6). In each case, the robot was given 10 attempts to climb the wall, and stopped each time it reached the top or fell. Slips that were recoverable were not counted as failures, although any recovery steps did not count towards the step total. A human teleoperator assisted with foothold selection during the swing phase and when necessary helped the robot maneuver free if it became caught on a rock. The vesicular basalt and slag surfaces were rearranged after 5 trials to increase the variety of terrain features. A summary of the results can be seen in Table II. The reported failure rate is the ratio of falls to steps taken, where each step equates to approximately 5cm of travel. The reported speed uses the fastest successful trial.

On cinderblock the robot was unable to maintain adhesion with the Intel NUC onboard, which reduces the adhesion margin by shifting the robot's center of mass away from the wall, so a smaller NVIDIA TX2 was carried instead as a placeholder. While flat surfaces like cinderblock are not the target environment for this robot, these trials allowed a controlled validation of the DIG strategy's efficacy. With this strategy, the robot saw a reduction in step failure rate from 6.4% to 2.3%. Qualitatively, the robot traversed the full 1 m wall in 6/10 trials vs 1/10 without the DIG forces.

The vesicular basalt trials were conducted with an older version of the robot with weaker AX-18A knee motors, so DIG forces could not be applied. Although the robot was able to climb with the NUC onboard, the failure rate was high

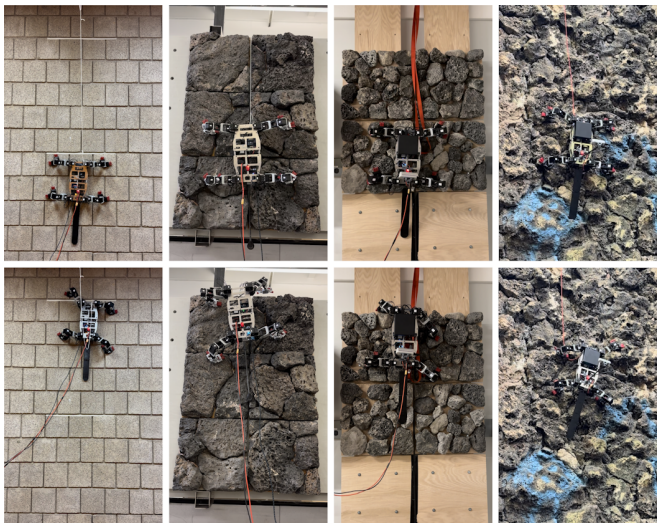

Fig. 6: From left to right: the LORIS robot prototype ascending cinderblock, vesicular basalt, slag, and tufa surfaces.

and the trials were instead conducted without an onboard computer or battery. The robot traversed the full 0.5 m in 4/10 trials, with a 6.4% step failure rate.

For the slag trials, the robot carried the NUC onboard and applied the DIG strategy. The robot traversed the full 0.5 m in 7/10 trials, with a 3.5% step failure rate. The ability to carry the full NUC is attributed to large-scale features of the slag surface which enable more robust grasps.

Finally, an outdoor field test was conducted on a bridge made of tufa stone (a variety of limestone) in a local park (Fig. 1). Although the highly irregular surface made suitable footholds hard to identify, LORIS managed to travel for 8 steps before failure. However, we were unable to conduct sufficient experiments at this location to produce an accurate failure rate measure.

V. Discussion

Although LORIS successfully traversed a variety of terrain types, its reliability is currently insufficient for real-world applications in which a single fall could be catastrophic. In both sets of cinderblock trials, the majority of failures were due to an individual gripper losing purchase. LORIS only has four grippers, one of which is typically in swing phase, so a single unexpected disengagement is often irrecoverable. In contrast, hexapedal robots like RiSE can keep five grippers engaged at all times – no single gripper failure can cause a fall. This redundancy compounds with the decreased load per gripper to explain much of the reliability discrepancy (RiSE traveled 9.6 m before failure on a stone aggregate surface [7], 4.4x further than LORIS averages on cinderblock).

On the remaining surfaces, spine engagement became significantly easier due to protruding features and the presence of large vesicles. Instead, the primary challenge came from footholds that were too highly curved for the gripper to conform easily. Other challenges included unexpected body collisions with the surface, and grippers snagging on rocks during both disengagement and the swing phase. In terms of climbing speed, a significant amount of time was spent

Surface	DIG	Payload	Total Mass (kg)	Failure Rate (failures/steps)	Speed (m/min)
Cinderblock	No	TX2	2.8	9/141 (6.4%)	0.29
Cinderblock	Yes	TX2	2.8	4/177 (2.3%)	0.22
Vesicular Basalt	No	None	2.1	6/94 (6.4%)	0.24
Slag	Yes	NUC	3.2	3/86 (3.5%)	0.20
Tufa	Yes	NUC	3.2	-	0.19

TABLE II: Climbing Experimental Results

selecting footholds and retrying steps if the gripper did not engage. Without these teleoperator interventions LORIS travels at 0.4 m/min, roughly double the current speed on slag. For these highly irregular environments, an effective foothold selection and path planning algorithm could dramatically improve both speed and reliability.

Despite these challenges, LORIS provides a valuable proof of concept as a lightweight robot that can nonetheless traverse unstructured vertical terrain. In particular, the directed inward grasping strategy has been shown to produce a significant increase in adhesion, reducing the failure rate on cinderblock by 64%. This comes at a small price in power consumption, raising the power draw during stance by 9.3% from roughly 51 to 56 W (of which the NUC draws 20 W).

VI. Conclusion

A splayed microspine gripper coupled with a passive wrist offers the potential for significant mass savings compared to fully actuated limbs with active grippers without sacrificing the ability to climb on irregular terrain. Important considerations for the design of such grippers include the carriage count, spacing, and wrist joint location, all of which can be optimized using the presented models. Equipping a robot with splayed grippers enables the generation of internal forces to improve adhesion, and a linear programming approach can be used in force control, foothold planning, or robot design to quickly and reliably determine the optimal force allocation. We validate the viability of this approach and the value of DIG force generation through controlled climbing experiments with a robot prototype on surfaces ranging from flat cinderblock to irregular slag. It is our hope that lightweight yet capable climbing robots like LORIS will pave the way for the first real-world deployments of robotic climbers on other worlds.

The robot prototype's current performance motivates a couple important directions of further research. One key challenge when climbing on irregular terrain is foothold selection – finding locations that are simultaneously the right shape to grasp, oriented well for generating contact forces, and relatively dense in asperities. Another approach would be the development of new gripper designs that can conform to a wider variety of terrain features without sacrificing performance on flat surfaces or requiring actuation. Finally, an under-utilized advantage of passive grippers is that they can engage with the surface nearly instantly, making them suitable for dynamic climbing gaits or maneuvers [25]. A robot using splayed grippers to carry out dynamic motions could offer increased energy efficiency, fall recovery, or even the ability to leap to a handhold that lies out of reach.

REFERENCES

[1] I. Baldwin, S. Kenig, A. Nicholas *et al.*, "Extreme science: Exploring the use of extreme-terrain rovers in Mars sample return," in *IEEE Aerospace Conference*, 2016, pp. 1–11.

[2] S. W. Squyres, A. H. Knoll, R. E. Arvidson *et al.*, "Exploration of Victoria Crater by the Mars rover Opportunity," *Science*, vol. 324, no. 5930, pp. 1058–1061, 2009.

[3] R. J. Léveillé and S. Datta, "Lava tubes and basaltic caves as astrobiological targets on Earth and Mars: A review," *Planetary and Space Science*, vol. 58, no. 4, pp. 592 – 598, 2010.

[4] I. A. Nesnas, L. Kerber, A. Parness *et al.*, "Moon Diver: a discovery mission concept for understanding the history of secondary crusts through the exploration of a lunar mare pit," in *IEEE Aerospace Conference*, 2019, pp. 1–23.

[5] A. T. Asbeck, S. Kim, W. R. Provancher *et al.*, "Scaling hard vertical surfaces with compliant microspine arrays," *Robotics Science and Systems Conference*, 2005.

[6] D. Schmidt and K. Berns, "Climbing robots for maintenance and inspections of vertical structures-a survey of design aspects and technologies," *Robotics and Autonomous Systems*, vol. 61, no. 12, pp. 1288–1305, 2013.

[7] M. J. Spenko, G. C. Haynes, J. A. Saunders *et al.*, "Biologically inspired climbing with a hexapedal robot," *Journal of Field Robotics*, vol. 25, no. 4-5, pp. 223–242, 2008.

[8] K. Carpenter, N. Wiltsie, and A. Parness, "Rotary microspine rough surface mobility," *IEEE/ASME Transactions on Mechatronics*, vol. 21, no. 5, pp. 2378–2390, 2016.

[9] S. Wang, H. Jiang, and M. R. Cutkosky, "Design and modeling of linearly-constrained compliant spines for human-scale locomotion on rocky surfaces," *The International Journal of Robotics Research*, vol. 36, no. 9, pp. 985–999, 2017.

[10] A. Parness, M. Frost, N. Thatte *et al.*, "Gravity-independent rock-climbing robot and a sample acquisition tool with microspine grippers," *Journal of Field Robotics*, vol. 30, no. 6, pp. 897–915, 2013.

[11] A. Parness, N. Abcouwer, C. Fuller *et al.*, "LEMUR 3: A limbed climbing robot for extreme terrain mobility in space," in *IEEE International Conference on Robotics and Automation*, 2017, pp. 5467–5473.

[12] P. Zi, K. Xu, Y. Tian, and X. Ding, "A mechanical adhesive gripper inspired by beetle claw for a rock climbing robot," *Mechanism and Machine Theory*, vol. 181, p. 105168, 2023.

[13] X. Li, W. Chen, X. Li *et al.*, "An underactuated adaptive microspines gripper for rough wall," *Biomimetics*, vol. 8, no. 1, 2023.

[14] K. Uno, N. Takada, T. Okawara *et al.*, "HubRobo: A lightweight multi-limbed climbing robot for exploration in challenging terrain," in *IEEE-RAS International Conference on Humanoid Robots*, 2021, pp. 209–215.

[15] Y. Tanaka, Y. Shirai, X. Lin *et al.*, "SCALER: A tough versatile quadruped free-climber robot," in *IEEE/RSJ International Conference on Intelligent Robots and Systems*, 2022, pp. 5632–5639.

[16] W. Ruotolo, F. S. Roig, and M. R. Cutkosky, "Load-sharing in soft and spiny paws for a large climbing robot," *IEEE Robotics and Automation Letters*, vol. 4, no. 2, pp. 1439–1446, 2019.

[17] L. R. Palmer III, E. Diller, and R. D. Quinn, "Toward gravity-independent climbing using a biologically inspired distributed inward gripping strategy," *IEEE/ASME Transactions on Mechatronics*, vol. 20, no. 2, pp. 631–640, 2015.

[18] G. C. Haynes, A. Khripin, G. Lynch *et al.*, "Rapid pole climbing with a quadrupedal robot," in *IEEE International Conference on Robotics and Automation*, 2009, pp. 2767–2772.

[19] K. A. Daltorio, T. C. Witushynsky, G. D. Wile *et al.*, "A body joint improves vertical to horizontal transitions of a wall-climbing robot," in *IEEE International Conference on Robotics and Automation*, 2008, pp. 3046–3051.

[20] A. T. Asbeck and M. R. Cutkosky, "Designing compliant spine mechanisms for climbing," *Journal of Mechanisms and Robotics*, vol. 4, p. 031007, 2012.

[21] A. Sintov, T. Avramovich, and A. Shapiro, "Design and motion planning of an autonomous climbing robot with claws," *Robotics and Autonomous Systems*, vol. 59, no. 11, pp. 1008–1019, 2011.

[22] P. Nadan, D. K. Patel, C. Pavlov *et al.*, "Microspine design for additive manufacturing," in *IEEE/RSJ International Conference on Intelligent Robots and Systems*, 2022, pp. 5640–5647.

[23] Y. Shirai, X. Lin, A. Schperberg *et al.*, "Simultaneous contact-rich grasping and locomotion via distributed optimization enabling free-climbing for multi-limbed robots," in *IEEE/RSJ International Conference on Intelligent Robots and Systems*, 2022, pp. 13 563–13 570.

[24] A. M. Johnson and D. E. Koditschek, "Legged self-manipulation," *IEEE Access*, vol. 1, pp. 310–334, May 2013.

[25] J. M. Brown, M. P. Austin, B. D. Miller, and J. E. Clark, "Evidence for multiple dynamic climbing gait families," *Bioinspiration & Biomimetics*, vol. 14, no. 3, p. 036001, 2019.